

# Force Output, Control of Film Structure, and Microscale Shape Transfer by Carbon Nanotube Growth under Mechanical Pressure

Anastasios John Hart\* and Alexander H. Slocum

*Department of Mechanical Engineering, Massachusetts Institute of Technology,  
77 Massachusetts Avenue, Room 3-470, Cambridge, Massachusetts 02139*

*Received December 5, 2005; Revised Manuscript Received February 24, 2006*

## ABSTRACT

We demonstrate that a film of vertically aligned multiwall carbon nanotubes (CNTs) can exert mechanical energy as it grows, and in our experiments the average force output is approximately 0.16 nN per CNT, for CNTs having an outer diameter of 9 nm and five walls. The film thickness after a fixed growth time and the alignment of CNTs within the film decrease concomitantly with increasing pressure which is applied by placing a weight on the catalyst substrate prior to growth, and CNTs grown under applied pressure exhibit significant structural faults. The measured mechanical energy density of CNT growth is significantly less than the energies of primary steps in the CNT formation process yet, based on the film volume, is comparable to the energy density of muscle and based on the volume of CNTs is comparable to hydraulic actuators. We utilize this principle to fabricate three-dimensional structures of CNTs which conform to the shape of a microfabricated template. This technique is a catalytic analogue to micromolding of polymer and metal microstructures; it enables growth of nanostructures in arbitrarily shaped forms having sloped surfaces and nonorthogonal corners and does not require patterning of the catalyst before growth.

While the chemical kinetics of carbon filament and carbon nanotube (CNT) growth by catalytic chemical vapor deposition (CVD) have been studied widely,<sup>1–8</sup> the effects of mechanical forces on CNT growth have only been explored using noncontact methods to guide the direction of growth. For example, isolated single wall nanotubes (SWNTs) can be grown to millimeter or centimeter lengths when suspended by gas flow during growth,<sup>9,10</sup> and application of an electric field during growth can exert a force on a nanotube and/or a catalyst particle,<sup>11</sup> to achieve aligned and direction-controllable growth in plasma-enhanced CVD processes<sup>12–14</sup> and to achieve growth of aligned CNTs spanning gaps between microfabricated electrodes.<sup>15</sup> Further, fluid flows and surface tension forces at fluid interfaces can direct postgrowth assembly of CNTs into patterns and structures on surfaces.<sup>16–18</sup>

We present a process for growing films of vertically aligned CNTs (VA-CNTs) under mechanical pressure, which affects the film microstructure and CNT wall structure, and facilitates measurement of the force which can be exerted collectively by large numbers of CNTs during growth. We use this principle to fabricate three-dimensional structures of CNTs which conform to the shape of a microfabricated template. This technique is analogous to microinjection or microtransfer molding,<sup>19–21</sup> where microstructures are fab-

ricated by flowing a precursor material such as a resin or powder into a microfabricated mold and subsequently curing the material. In our process, a gaseous feedstock is catalytically transformed into CNTs within the mold, filling the cavities with a scaffold of solid nanostructures which is embossed by the mold as mechanical pressure builds during CNT growth within the cavities.

Our previous work in VA-CNT film growth<sup>22</sup> demonstrates that placement of a piece of silicon wafer as a “cap” on top of the growth substrate moderates the gas flow to the catalyst, and the VA-CNT film lifts the cap as it grows. Other studies show that CNT growth can lift a film which is deposited on top of the catalyst<sup>23,24</sup> and that stacked CNT multilayers can be grown when catalyst is intermittently supplied to the catalyst–substrate interface, where each additional layer lifts the previously grown layers.<sup>25,26</sup> Here we provide the first indication of mechanochemical effects<sup>27</sup> on CNT growth reactions, where a mechanical force applied to the growth site affects the morphology and growth rate of CNTs in a densely packed film. Film growth under mechanical pressure may be suitable for a wide variety of nanostructures in addition to CNTs, such as inorganic and semiconducting nanowires, and CNT layers with controlled structure and permeability are useful for applications in electrochemical energy storage, membranes and electrodes in fuel cells, and fluid filtration.<sup>28,29</sup>

\* To whom correspondence may be addressed. E-mail: ajhart@mit.edu.

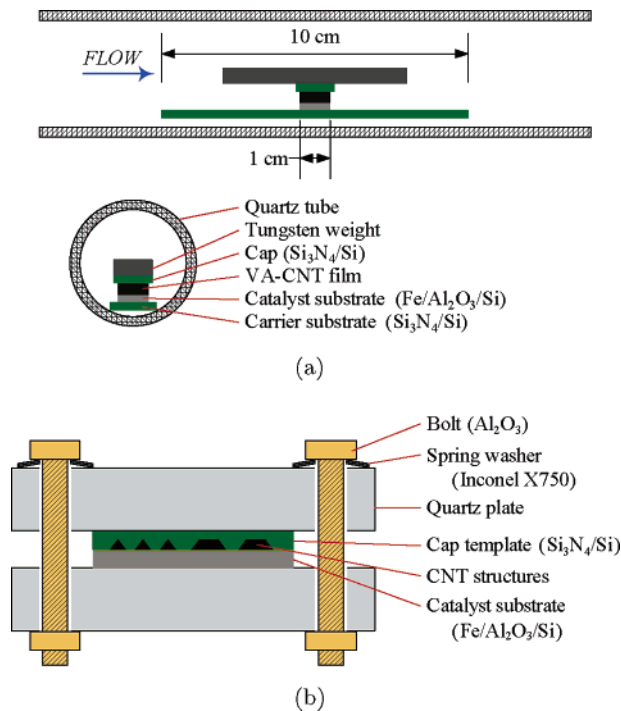


**Figure 1.** Substrate configurations for applying static forces on CNT films during growth: (a) placement of a catalyst-coated substrate under tungsten weight, where growth lifts the tungsten weight; (b) clamping a catalyst substrate against a microstructured template, where CNTs grow to fill the cavities in the template.

We conduct CNT “weightlifting” experiments by placing a  $1 \times 1$  cm silicon substrate (p-type, 1–10  $\Omega$  cm, Silicon Quest International) coated with a 1.2/10 nm Fe/Al<sub>2</sub>O<sub>3</sub> film deposited by electron beam evaporation, under a tungsten weight as shown in Figure 1a. The catalyst surface is separated from the weight by a Si<sub>3</sub>N<sub>4</sub>-coated silicon cover which is slightly larger than the substrate, and the nonpolished surface ( $R_a \approx 150$  nm) of the cover is in initial contact with the catalyst film. The weight is a stack of coupons (1 cm  $\times$  3–9 cm) which are cut from a tungsten sheet (99.95+%, Midwest Tungsten) using an abrasive waterjet (Omax), and then sonicated in acetone and rinsed with deionized (DI) H<sub>2</sub>O. Incidentally, patches of tangled and aligned CNTs are also grown on the waterjet-cut edges of the tungsten weights, possibly due to inclusion of micro-particles of garnet abrasive from the cutting process. However, placing a tungsten coupon immediately upstream of the growth substrate does not affect the characteristics of the CNT film grown from the Fe/Al<sub>2</sub>O<sub>3</sub>/Si substrate.

For physically templated growth, the catalyst-coated substrate is clamped against a microfabricated silicon template using a quartz fixture as drawn in Figure 1b, and the assembly is preloaded using Al<sub>2</sub>O<sub>3</sub> bolts and high-temperature spring washers. The template is fabricated by standard photolithography and etching using aqueous KOH (20 wt % in DI H<sub>2</sub>O, 80 °C). The pattern is etched on the nonpolished side of the wafer to prevent bonding of the template to the growth substrate during the shape transfer process.

CNT growth is performed in a single-zone atmospheric pressure quartz tube furnace (Lindberg). The furnace temperature is ramped under 400 sccm Ar. Flows of 100/500/

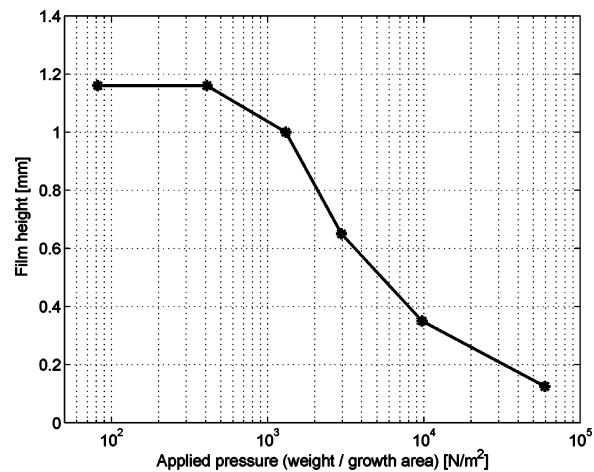


**Figure 2.** Measured relationship between CNT film height and pressure applied during growth, for 15 min of growth.

200 sccm C<sub>2</sub>H<sub>4</sub>/H<sub>2</sub>/Ar (99.5/99.999/99.999%, Airgas) are maintained for the growth period of 15 min, and the flows of Ar and H<sub>2</sub> used during growth are established 1 min prior to C<sub>2</sub>H<sub>4</sub>. Characterization is performed by scanning electron microscopy (SEM) using a Philips XL30-FEG-ESEM at 5keV, and by high-resolution transmission electron microscopy (HRTEM) using a JEOL-2011 at 200 keV with samples dispersed gently in 2-propanol and dried on a holey carbon grid (Quantifoil). An “average” CNT from our process has an outer diameter of 9 nm and five walls, as observed by TEM imaging. The films contain approximately  $1.5 \times 10^{10}$  CNTs/cm<sup>2</sup>. This is calculated using the mass of an average CNT (based the dimensions measured by TEM and the density of graphite), the film volume which is estimated by SEM imaging, and the film mass determined by weighing the film using a thermogravimetric analyzer (TGA, Perkin-Elmer) at room temperature.

The growing VA-CNT film lifts the tungsten weight upward, demonstrating that CNT growth exerts an extrusive force. Figure 2 plots the final thickness of the VA-CNT film, versus the applied pressure, at otherwise identical CVD conditions. The thickness of the VA-CNT film and the degree of alignment within the film decrease with increasing applied pressure, beyond a minimum pressure which is needed to suppress nonuniformities in the film which emerge in regions that grow at a relatively rapid rate. For these slight pressures ( $\leq 500$  N/m<sup>2</sup>;  $\leq 1$  g), we observe no uniform effect of pressure on growth. The weight rests on the peaks of the top surface of the film, which has a waviness of approximately 20% ( $\approx 200$   $\mu$ m) of the total thickness. For higher pressures, the film thickness decreases in an approximately linear fashion with the logarithm of applied pressure, and the top surface of the film is substantially flat (Figure 3a, bottom). With increasing pressure beyond the threshold, the internal structure of the CNT films changes from well aligned (Figure 3b), to less aligned (Figure 3d), to “collapsed” or “serpentine” pattern, where a sample grown under 60 000 N/m<sup>2</sup> pressure exhibits a spatial wavelength of  $\approx 300$  nm (Figure 3d). We observe that the wavelength of the film structure is smaller for higher applied pressures; however, further study is necessary to quantify this relationship in detail.

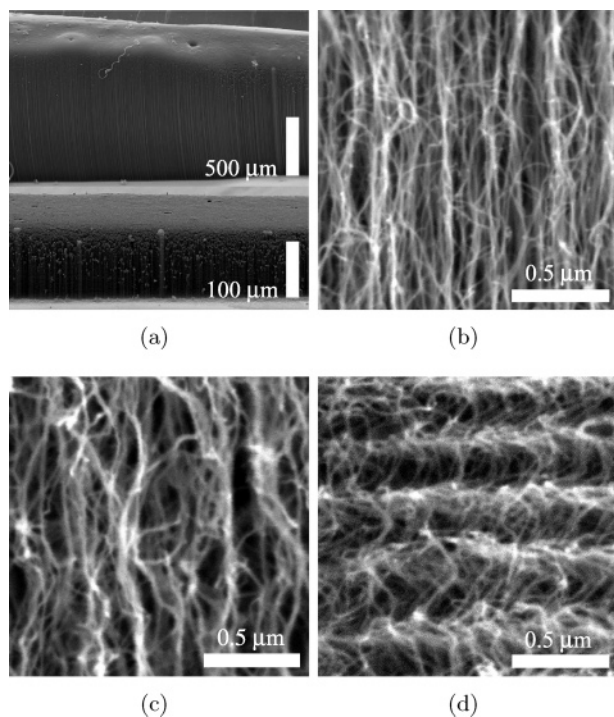


**Figure 3.** Morphology of CNT films grown under different applied pressures: (a) sidewall of film grown under a 0.2 g weight (top) and a 61 g weight (bottom); (b) alignment within film grown under a 0.2 g silicon weight ( $\approx 80 \text{ N/m}^2$ ); (c) grown under a 6 g tungsten weight ( $\approx 3000 \text{ N/m}^2$ ); (d) grown under a 61 g tungsten weight ( $\approx 60\,000 \text{ N/m}^2$ ).

TEM imaging (Figure 4) reveals that mechanical pressure causes the CNTs to have a prevalence of significant structural faults and kinks in the CNT sidewalls, compared to relatively straight CNTs which are more abundant in aligned films grown under little or no mechanical pressure. Isolated groups of CNTs show the serpentine CNT shape (Figure 4d) which is microscopically realized within the collapsed films. Microscopic curves in the CNTs are accommodated by the sharp faults in the sidewalls and local changes in the inner and outer diameters, rather than by smooth curves in the lattice. Generally, the structure of CNTs grown under mechanical pressure is different than the structure of a CNT, which is deformed after growth.<sup>30,31</sup> Oblique forces on the catalyst particle may cause different rates of carbon precipitation across the catalyst particle, causing the observed defects in the wall structure.<sup>32</sup>

In the “capped” sample configuration (Figure 1a), the gas flow to catalyst is restricted by the cap and gas reaches the catalyst by diffusing between the cap and substrate. As a result, VA-CNT growth occurs only around the periphery of the substrate (Figure S1), in an area where the initial gas supply is sufficient to activate growth in a vertically aligned conformation. For a  $1 \times 1 \text{ cm}^2$  substrate, the area of VA-CNT growth is typically  $0.1\text{--}0.2 \text{ cm}^2$ , and we calculate the applied pressure for each experiment by dividing the weight placed on the cap by the area of VA-CNT growth which is measured by SEM examination at low magnification. The area of VA-CNT growth necessarily fluctuates from run-to-run because of debris which establishes a slight initial gap between the catalyst substrate and the cap, and therefore

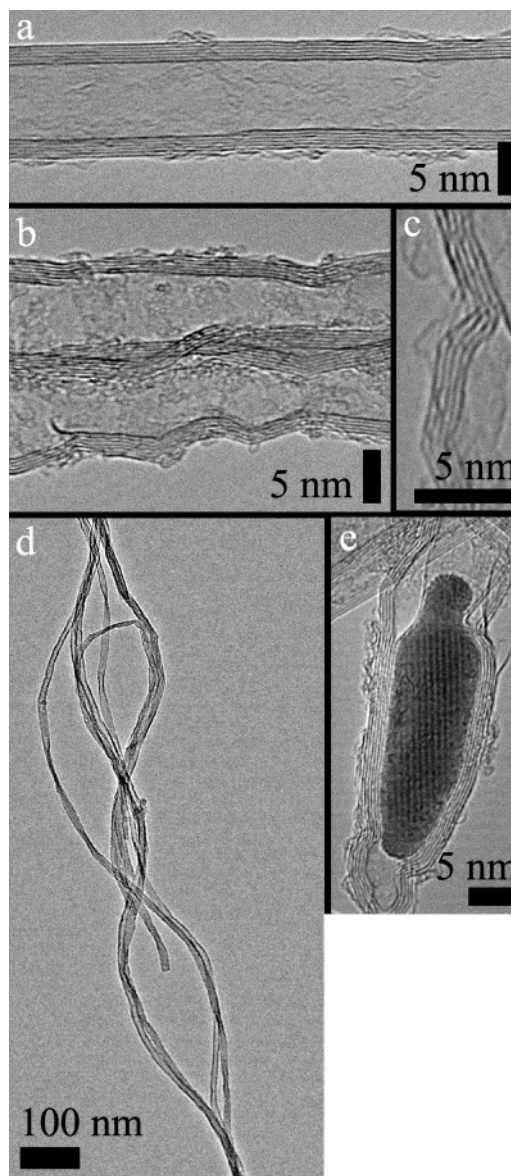


**Figure 4.** TEM images: (a) typically straight multiwall CNT from aligned film; (b) defective CNTs with sidewall kinks and ripples, which are abundant in films grown under high applied pressure; (c) close-up of defective sidewall structure; (d) low-magnification image of “serpentine” CNTs isolated from film having collapsed microstructure, grown under  $60\,000 \text{ N/m}^2$  pressure, showing abundant sidewall defects and local changes in diameter; (e) Fe catalyst particle encapsulated at bottom end of CNT.

modulates the amount of gas which initially diffuses into the gap to initiate VA-CNT growth. However, the thickness of the VA-CNT region is invariant among many identical experiments in the capped configuration and in different sample configurations,<sup>22</sup> confirming that the flow restriction introduced by the cap does not affect the steady growth rate.

Because applied pressure causes the CNTs in a film to be more closely packed, hindrance of gas diffusion through the film<sup>5,6</sup> may contribute to the slower observed growth of CNTs under applied pressure. To evaluate this hypothesis, we also grew CNTs from lithographically patterned samples where the catalyst is arranged so CNTs grow in regularly spaced “pillars”, so diffusion of gas to the catalyst is limited only

**Table 1.** Comparison of Mechanical Energy Output by CNT Growth to Estimated Energies Involved in CNT Formation

force exerted per CNT during growth	$1.6 \times 10^{-10}$	nN
mechanical energy output per CNT	$1.5 \times 10^{-4}$	eV/atom
free surface energy of a single CNT at 1023 K	$3.9 \times 10^{-3}$	eV/atom
elastic strain energy stored in a single CNT	$1.4 \times 10^{-2}$	eV/atom
measured activation energy of reaction	1.40	eV/atom

by the half-width of the pillar cross section, rather than the thickness of the film or the distance from the outer edge of the sample. For example, under equivalent applied pressures, an array of  $200 \times 200 \mu\text{m}$  pillars grows to approximately the same effective height as a sample having a uniform film of catalyst (Figure S2), suggesting that mechanical constraint rather than diffusion limitation plays a dominant role in decreasing the growth rate of CNTs in our experiments.

Further, while the CNT length is approximately equal to the film thickness for a well-aligned film, the length of CNTs in a collapsed film substantially exceeds the film thickness. For example, in the film grown under  $60\,000 \text{ N/m}^2$  pressure (Figure 3d), the CNT length is 40% (assuming an in-plane “zig-zag”) to 90% (assuming the CNTs are helices) greater than the film thickness. Still, the “effective” CNT length, accounting for the collapsed microstructure, decreases significantly with applied pressure.

When a CNT film lifts a weight, the force exerted per CNT ( $F_{\text{CNT}}$ ) is

$$F = \frac{mg}{N_{\text{CNT}}A_{\text{G}}}$$

where  $m$  is the mass of the tungsten weight,  $g$  is the gravitational constant,  $N_{\text{CNT}}$  is the number of CNTs per unit area of vertically aligned film ( $1.5 \times 10^{10} \text{ CNTs/cm}^2$ ), and  $A_{\text{G}}$  is the area of vertically aligned growth on the substrate. The value of  $F$  is computed for each experiment in the data set (Figure 2) and averaged to give a representative value of 0.16 nN per CNT for our process. This is equivalent to a mechanical energy of 0.16 nJ per meter of CNT growth, or  $2.4 \times 10^{-4} \text{ eV/atom}$ .

Table 1 compares the average mechanical energy exerted to estimated energies of processes involved in CNT formation. The total surface energy of the graphite layers on the inner and outer walls of a CNT, which are created when the CNT evolves from the catalyst particle, is

$$U_{\text{surface}} = \sigma_{\text{g}}\pi L(d_{\text{o}} + d_{\text{i}}) \quad (2)$$

where  $d_{\text{o}}$  is the outer diameter of the CNT,  $d_{\text{i}}$  is the inner diameter, and  $\sigma_{\text{g}}$  is the surface energy of graphite ( $0.089 \text{ J/m}^2$ , see Supporting Information).<sup>33</sup> The strain energy required to bend a stack of graphene sheets into the cylindrical shape of a CNT is<sup>34</sup>

$$U_{\text{strain}} = \frac{\pi E_{\text{g}}\delta_{\text{g}}^2 L}{12} \ln \frac{d_{\text{o}}}{d_{\text{i}}} \quad (3)$$

where  $E_{\text{g}} = 1 \times 10^{10} \text{ N/m}^2$  is assumed for the Young’s

modulus of graphite and  $\delta_{\text{g}} = 3.4 \times 10^{-10} \text{ m}$  is the interlayer spacing between layers. While the catalytic growth process does not necessarily exert this energy because a CNT does not form by bending graphite into a cylinder, this quantity gives a measure of the mechanical energy which would be released if a CNT were cut along its length after growth and, therefore, is the mechanical energy potential in a CNT. The activation energy for our growth reaction is 1.4 eV/atom, as estimated by an Arrhenius method<sup>7,35</sup> from the dependence of growth rate on temperature.

The mechanical energy exerted by growth is 1 to 4 orders of magnitude less than the other estimated energies, further suggesting that the observed change in film microstructure at relatively high applied pressures is governed by a finer effect of force on the production of defects as observed by TEM imaging. We believe the ordered serpentine arrangement in the films grown under pressure is influenced by lateral constraint introduced by neighboring CNTs. This space also gives the CNTs room to “wiggle” near the catalyst, allowing the direction of growth to change in concert with production of structural faults. The serpentine morphology is similar to previously observed multimode buckling of high-aspect-ratio micromachined beams<sup>36</sup> and laterally constrained plates.<sup>37</sup> Further, postgrowth foamlike compressibility of VA-MWNT films grown from a liquid hydrocarbon feedstock has been attributed to coordinated multimode buckling of the CNTs, where the CNT film collapses into a reversible serpentine-like arrangement upon application of a compressive load.<sup>38</sup> We observe significant irreversible compressibility of our films when compacted following growth and are studying the postgrowth mechanical properties of our CNT films in further detail.

Single-mode buckling of a CNT after growth can be modeled by treating the CNT as an Euler column.<sup>39,40</sup> On the basis of this calculation (see Supporting Information) the CNT length for a buckling force of 0.40 nN is  $\approx 2 \mu\text{m}$  (for 9 nm o.d., five layers), which far exceeds the 300 nm wavelength of the serpentine morphology which is observed after growth under this force (Figure 3d). Alternatively, approximately 10 nN would be required to buckle a CNT over 300 nm. The large discrepancy between the force exerted during growth and the force which may be required to create a similar structure by postgrowth deformation suggests that a larger force is needed to deform CNTs after growth than during growth. This hypothesis is qualitatively confirmed by an experiment where we place the catalyst substrate under a weight, yet initially space the substrate from the weight so a uniform and well-aligned film grows before contacting the template. The resulting film (Figure S3) has a well-aligned upper region and a collapsed lower region, where the wavelength of the pattern in the collapsed region

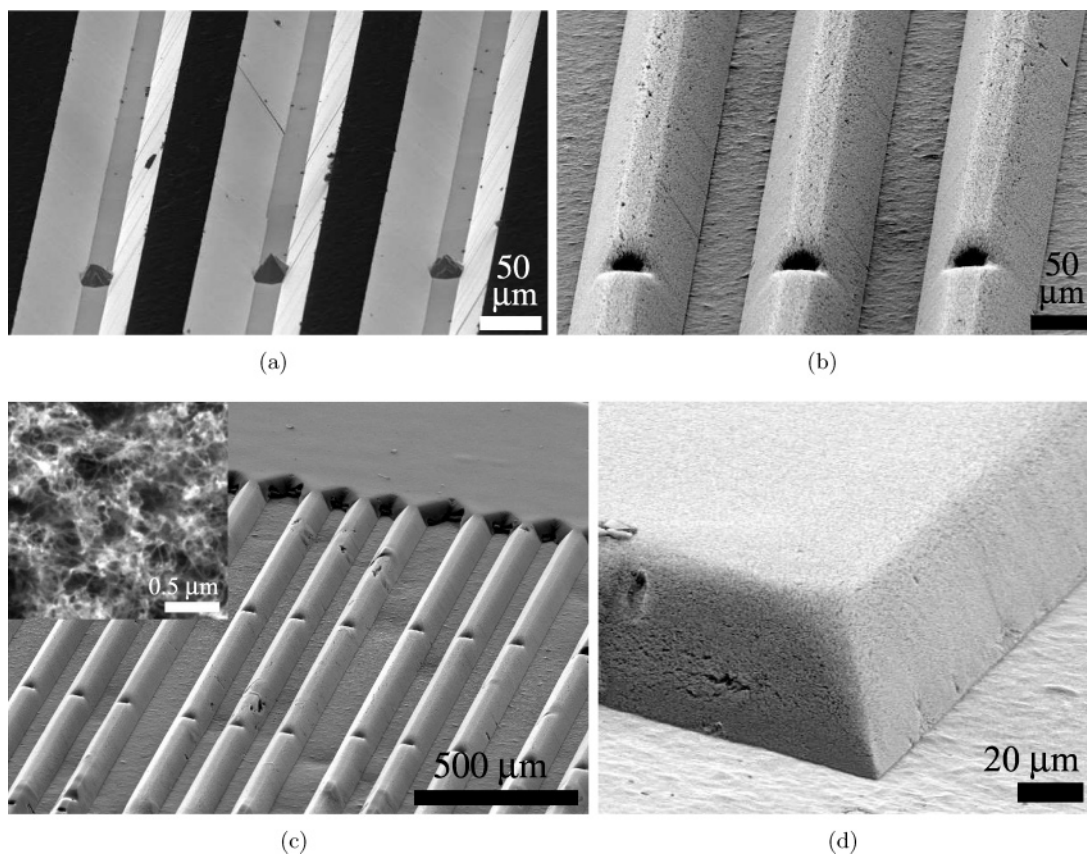


**Figure 5.** Growth of CNT microforms: (a) KOH-etched trapezoidal microchannel template with included pyramidal islands; (b) CNT microforms grown to fill and conform to template; (c) broad area of microforms (scale  $500\ \mu\text{m}$ ), with inset showing typical outer surface of a microform; (d) close view of concave corner, showing sharply angled transition at interface of microform and substrate, and rounding of corner.

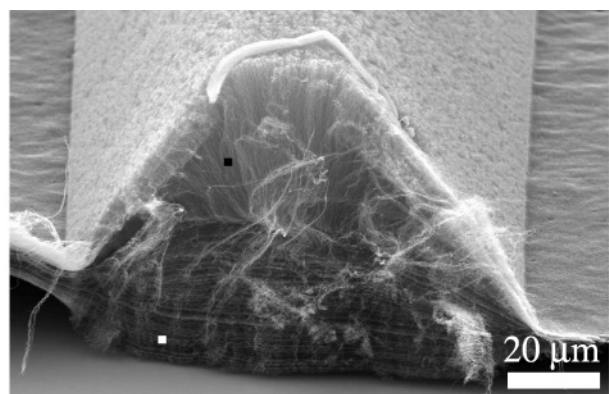
decreases toward the bottom of the film. Mechanical resistance is introduced when the top of the film contacts the template, and this resistance is transmitted through the film to the base where the growth sites exert an opposing force, which slows and perhaps eventually terminates growth.

We utilize the force output capability of CNT growth to physically template three-dimensional CNT microforms by a “catalytic micromolding” approach. Figure 5 shows CNT structures which are grown to replicate an etched silicon template which is held against the catalyst-coated substrate during CNT growth. The  $\text{C}_2\text{H}_4/\text{H}_2/\text{Ar}$  mixture diffuses into the cavities between the template and the growth substrate. The template is cleanly removed following growth, leaving the free-standing structures on the growth substrate, and the template is then reused. This technique surpasses traditional methods for growing CNT microstructures using two-dimensional catalyst patterns on substrates,<sup>41–44</sup> allowing fabrication of arbitrary shapes having sloped and/or curved surfaces and nonorthogonal corners, and does not require patterning of the catalyst. In our initial experiments, concave corners of the microform (convex corners of the template) are sharper than convex corners and yet are rounded to  $5\text{--}10\ \mu\text{m}$  (Figure 5d). The finest replication we have attempted is a  $5\ \mu\text{m}$  wide KOH-etched microchannel with triangular cross sections, and the apex of such a microform is rounded to  $\approx 2\ \mu\text{m}$ . The accuracy and resolution of shape replication depend on the density of CNTs growing from the substrate

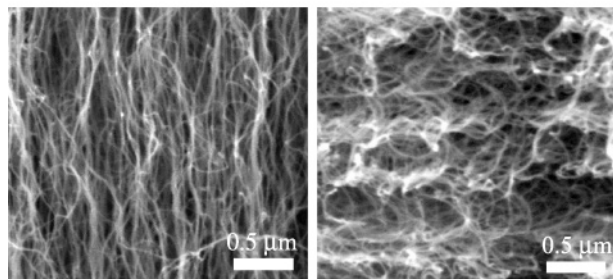
and on the gas flow through the template. With appropriate and uniform gas flow, such as by using a porous template, these structures could be fabricated over large substrate areas. Further, application of an electric field between the growth substrate and template may help guide the CNTs into especially narrow template features and sharp corners, achieving shape transfer at a significantly higher resolution than that demonstrated by our initial results.

Sectioning a CNT microform reveals how its structure evolves under mechanical constraint during growth, as shown in Figure 6. Initially, a well-aligned CNT film grows upward into the cavity between the substrate and template. When a portion of the film reaches the template surface, compressive forces are transmitted to the bases of these CNTs. Because the film cannot freely move upward, CNTs begin to “bunch up” with additional growth at the base of the structure. In this example, the slanted sidewalls “pin” growth from the outer edges of the cross section, finally leaving a densely collapsed region in the lower half of the microform and an aligned region in the upper half of the microform.

Our measurements demonstrate that CNT growth can exert a considerable extrusive force, which can be balanced by pressure exerted by an external template or by mechanical constraint from neighboring CNTs within the film. A CNT film can lift tens of thousands of times its own weight as it grows, evoking thoughts of fire ants which can lift “only” 50 times their own weight. Although CNT film growth is

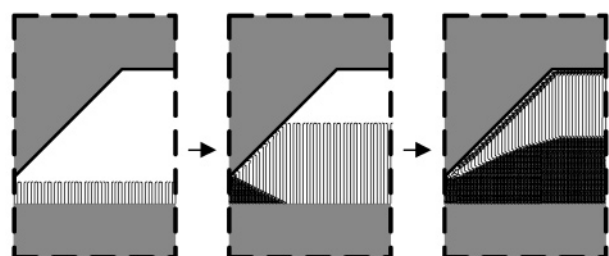


(a)



(b)

(c)



(d)

**Figure 6.** Cross section of trapezoidal-channel CNT microform: (a) full view, showing crowding of CNTs at bottom, which is induced by continued base growth after CNTs initially fill the form; (b) close view of aligned region near top of cross section (at black square in (a)); (c) close view of collapsed region near bottom of cross section (at white square in (a)); (d) simplified illustration of how the internal structure of a microform evolves under mechanical constraint during the growth process.

an impractical actuation technique because of its operating temperature, low speed, and irreversibility, the measured energy density based on the volume of the CNT film is  $2.4 \times 10^4 \text{ J/m}^3$ , which is comparable to muscle. The energy density based on the mass of CNTs is  $3.0 \times 10^3 \text{ J/kg}$ , which is comparable to shape memory alloys, and based on the volume of a hexagonally packed arrangement of such CNTs is  $2.8 \times 10^6 \text{ J/m}^3$ , which is comparable to hydraulic actuators.<sup>45,46</sup> This may warrant new applications for CNTs in microelectromechanical systems which take advantage of force output and actuation capability, such as for initiating folding of microstructures,<sup>47</sup> for embedding CNT layers as constrained energy dissipators,<sup>48</sup> or for reducing thermal or electrical contact resistance by direct growth or physical

templating of conformal CNT film structures at interfaces between components. Going forward, studying the force output of CNT growth as it depends on the growth conditions and density of CNTs in a film may give a more complete understanding of the reaction energetics, particularly of how compressive or tensile forces affect the production of defects in CNT structures during growth from catalytic particles by CVD.

**Acknowledgment.** This work was funded by NSF Grant No. DMI-0521985, and by an Ignition Grant from the MIT Deshpande Center for Technological Innovation. A. J. Hart is grateful for a Fannie and John Hertz Foundation Fellowship. Thanks to Y. M. Chiang of the MIT DMSE for sharing his laboratory.

**Supporting Information Available:** Calculations of buckling forces and actuation energies, a detailed table of estimated energy values, SEM images of growth pattern around the perimeter of the substrate, SEM images of CNT pillars grown under mechanical pressure, SEM images of a CNT film grown in contact with a flat and weighted template. This material is available free of charge via the Internet at <http://pubs.acs.org>.

## References

- (1) Baker, R. T. K.; Harris, P. S.; Thomas, R. B.; Waite, R. J. *J. Catal.* **1973**, *30*, 86–95.
- (2) Tibbetts, G. G. *J. Cryst. Growth* **1985**, *73*, 431–438.
- (3) Tibbetts, G. G.; Devour, M. G.; Rodda, E. J. *Carbon* **1987**, *25*, 367–375.
- (4) Jablonski, G. A.; Geurts, F. W. A. H.; Sacco, A. *Carbon* **1992**, *30*, 99–106.
- (5) Louchev, O. A.; Laude, T.; Sato, Y.; Kanda, H. *J. Chem. Phys.* **2003**, *118*, 7622–7634.
- (6) Poretzky, A. A.; Geohegan, D. B.; Jesse, S.; Ivanov, I. N.; Eres, G. *Appl. Phys. A* **2005**, *81*, 223–240.
- (7) Liu, K.; Jiang, K.; Feng, C.; Chen, Z.; Fan, S. *Carbon* **2005**, *43*, 2850–2856.
- (8) Futaba, D.; Hata, K.; Yamada, T.; Mizuno, K.; Yumura, M.; Iijima, S. *Phys. Rev. Lett.* **2005**, *95*.
- (9) Huang, S. M.; Cai, X. Y.; Liu, J. *J. Am. Chem. Soc.* **2003**, *125*, 5636–5637.
- (10) Zheng, L. *Nat. Mater.* **2004**, *3*, 673–676.
- (11) Merkulov, V. I.; Melechko, A. V.; Guillorn, M. A.; Lowndes, D. H.; Simpson, M. L. *Appl. Phys. Lett.* **2001**, *79*, 2970–2972.
- (12) Bower, C.; Zhu, W.; Jin, S. H.; Zhou, O. *Appl. Phys. Lett.* **2000**, *77*, 830–832.
- (13) Chowalla, M.; Teo, K. B. K.; Ducati, C.; Rupasinghe, N. L.; Amaratunga, G. A. J.; Ferrari, A. C.; Roy, D.; Robertson, J.; Milne, W. I. *J. Appl. Phys.* **2001**, *90*, 5308–5317.
- (14) AuBuchon, J. F.; Chen, L. H.; Gapin, A. I.; Kim, D. W.; Daraio, C.; Jin, S. H. *Nano Lett.* **2004**, *4*, 1781–1784.
- (15) Zhang, Y. G.; Chang, A. L.; Cao, J.; Wang, Q.; Kim, W.; Li, Y. M.; Morris, N.; Yenilmez, E.; Kong, J.; Dai, H. *J. Appl. Phys. Lett.* **2001**, *79*, 3155–3157.
- (16) Ko, H.; Peleshanko, S.; Tsukruk, V. V. *J. Phys. Chem. B* **2004**, *108*, 4385–4393.
- (17) Tsukruk, V. V.; Ko, H.; Peleshanko, S. *Phys. Rev. Lett.* **2004**, *92*, 065502.
- (18) Chakrapani, N.; Wei, B. Q.; Carrillo, A.; Ajayan, P. M.; Kane, R. S. *Proc. Natl. Acad. Sci. U.S.A.* **2004**, *101*, 4009–4012.
- (19) Kim, E.; Xia, Y.; Whitesides, G. M. *Nature* **1995**, *376*, 581–584.
- (20) Zhao, X. M.; Xia, Y. N.; Whitesides, G. M. *Adv. Mater.* **1996**, *8*, 837–840.
- (21) Piottter, V.; Bauer, W.; Benzler, T.; Emde, A. *Microsyst. Technol.* **2001**, *7*, 99–102.
- (22) Hart, A. J.; Slocum, A. H. *J. Phys. Chem. B* **2006**, *110*, DOI: 10.1021/jp055498b.

- (23) Wei, B. Q.; Zhang, Z. J.; Ramanath, G.; Ajayan, P. M. *Appl. Phys. Lett.* **2000**, *77*, 2985–2987.
- (24) Chen, Z. X.; Merikhi, J.; Koehler, I.; Bachmann, P. K. *Diamond Relat. Mater.* **2006**, *15*, 104–108.
- (25) Li, X. S.; Cao, A. Y.; Jung, Y. J.; Vajtai, R.; Ajayan, P. M. *Nano Lett.* **2005**, *5*, 1997–2000.
- (26) Pinault, M.; Pichot, V.; Khodja, H.; Launois, P.; Reynaud, C.; Mayne-L’Hermite, M. *Nano Lett.* **2005**, *5*, 2394–2398.
- (27) Beyer, M.; Clausen-Schaumann, H. *Chem. Rev.* **2005**, *105*, 2921–2948.
- (28) Che, G. L.; Lakshmi, B. B.; Fisher, E. R.; Martin, C. R. *Nature* **1998**, *393*, 346–349.
- (29) Srivastava, A.; Srivastava, O. N.; Talapatra, S.; Vajtai, R.; Ajayan, P. M. *Nat. Mater.* **2004**, *3*, 610–614.
- (30) Iijima, S.; Brabec, C.; Maiti, A.; Bernholc, J. *J. Chem. Phys.* **1996**, *104*, 2089–2092.
- (31) Poncharal, P.; Wang, Z. L.; Ugarte, D.; de Heer, W. A. *Science* **1999**, *283*, 1513–1516.
- (32) Amelinckx, S.; Zhang, X. B.; Bernaerts, D.; Zhang, X. F.; Ivanov, V.; Nagy, J. B. *Science* **1994**, *265*, 635–639.
- (33) Abrahamson, J. *Carbon* **1973**, *11*, 337–362.
- (34) Tibbetts, G. G. *J. Cryst. Growth* **1984**, *66*, 632–638.
- (35) Chorkendorff, I.; Niemantsverdriet, J. W. *Concepts of modern catalysis and kinetics*; Wiley-VCH: Weinheim, Germany, 2003.
- (36) Carr, S. M.; Lawrence, W. E.; Wybourne, M. N. *Europhys. Lett.* **2005**, *69*, 952–958.
- (37) Roman, B.; Pocheau, A. *Europhys. Lett.* **1999**, *45*, 602–608.
- (38) Cao, A.; Dickrell, P. L.; Sawyer, W. G.; Ghasemi-Nejhad, M. N.; Ajayan, P. M. *Science* **2005**, *310*, 1307–1310.
- (39) Akita, S.; Nishijima, H.; Kishida, T.; Nakayama, Y. *Jpn. J. Appl. Phys.* **2000**, *39*, 3724–3727.
- (40) Hibbeler, R. C. *Statics and Mechanics of Materials*; Prentice Hall: Englewood Cliffs, NJ, 1993.
- (41) Terrones, M.; Grobert, N.; Olivares, J.; Zhang, J. P.; Terrones, H.; Kordatos, K.; Hsu, W. K.; Hare, J. P.; Townsend, P. D.; Prassides, K.; Cheetham, A. K.; Kroto, H. W.; Walton, D. R. M. *Nature* **1997**, *388*, 52–55.
- (42) Fan, S. S.; Chapline, M. G.; Franklin, N. R.; Tomblor, T. W.; Cassell, A. M.; Dai, H. J. *Science* **1999**, *283*, 512–514.
- (43) Kind, H.; Bonard, J. M.; Emmenegger, C.; Nilsson, L. O.; Hernadi, K.; Maillard-Schaller, E.; Schlapbach, L.; Forro, L.; Kern, K. *Adv. Mater.* **1999**, *11*, 1285–1289.
- (44) Hata, K.; Futaba, D. N.; Mizuno, K.; Namai, T.; Yumura, M.; Iijima, S. *Science* **2004**, *306*, 1362–1364.
- (45) Huber, J. E.; Fleck, N. A.; Ashby, M. F. *Proc. R. Soc. London* **1997**, *453*, 2185–2205.
- (46) Zupan, M.; Ashby, M. F.; Fleck, N. A. *Adv. Eng. Mater.* **2002**, *4*, 933–940.
- (47) Arora, W.; Nichol, A.; Smith, H.; Barbastathis, G. *Appl. Phys. Lett.* **2006**, *88*, 053108.
- (48) Rajoria, H.; Jalili, N. *Compos. Sci. Technol.* **2005**, *65*, 2079–2093.

NL0524041